Mitochondrial degeneration and not apoptosis is the primary cause of embryonic lethality in ceramide transfer protein mutant mice

Xin Wang,[1] Raghavendra Pralhada Rao,[1] Teresa Kosakowska-Cholody,[1] M. Athar Masood,[2] Eileen Southon,[4] Helin Zhang,[5] Cyril Berthet,[4] Kunio Nagashim,[3] Timothy K. Veenstra,[2] Lino Tessarollo,[4] Usha Acharya,[6] and Jairaj K. Acharya[1]

[1]Laboratory of Cell and Developmental Signaling, [2]Laboratory of Proteomics and Analytical Technologies, and [3]Electron Microscopy Facility, Science Applications International Corporation–Frederick, Inc., and [4]Mouse Cancer Genetics Program, National Cancer Institute at Frederick, Frederick, MD 21702
[5]Marlene Stewart Greenebaum Cancer Center, University of Maryland School of Medicine, Baltimore, MD 21201
[6]Program in Gene Function and Expression, University of Massachusetts Medical School, Worcester, MA 01605

Ceramide transfer protein (CERT) functions in the transfer of ceramide from the endoplasmic reticulum (ER) to the Golgi. In this study, we show that CERT is an essential gene for mouse development and embryonic survival and, quite strikingly, is critical for mitochondrial integrity. CERT mutant embryos accumulate ceramide in the ER but also mislocalize ceramide to the mitochondria, compromising their function. Cells in mutant embryos show abnormal dilation of the ER and degenerating mitochondria. These subcellular changes manifest as heart defects and cause severely compromised cardiac function and embryonic death around embryonic day 11.5. In spite of ceramide accumulation, CERT mutant mice do not die as a result of enhanced apoptosis. Instead, cell proliferation is impaired, and expression levels of cell cycle–associated proteins are altered. Individual cells survive, perhaps because cell survival mechanisms are activated. Thus, global compromise of ER and mitochondrial integrity caused by ceramide accumulation in CERT mutant mice primarily affects organogenesis rather than causing cell death via apoptotic pathways.

Introduction

Sphingolipids are important structural elements of cell membranes and provide mechanical and chemical stability (Acharya and Acharya, 2005; Riezman, 2006; Zeidan and Hannun, 2007; Hannun and Obeid, 2008). They also serve specific functions in cell–cell recognition and signaling (English et al., 2002; Futerman and Hannun, 2004; Hla, 2005; Zheng et al., 2006). Several intermediates of the sphingolipid metabolic pathway are known as second messengers that mediate processes such as angiogenesis, cell growth, differentiation, and apoptosis (Merrill, 2002; Alvarez et al., 2007; Haberkant et al., 2008; van Meer et al., 2008). Ceramide is a precursor for the synthesis of several sphingolipids. In addition to being an obligate intermediate in the de novo sphingolipid biosynthetic pathway, ceramide has been implicated as a mediator of stress responses, cell differentiation, and apoptosis (Hannun and Obeid, 2008). Its involvement in apoptosis is clinically significant: many chemotherapeutic agents for cancer appear to induce ceramide-dependent apoptosis, and some of the associated enzymes and proteins, including ceramide transfer protein (CERT), are being investigated as targets for cancer therapies (Ogretmen and Hannun, 2004; Savtchouk et al., 2007; Swanton et al., 2007; Zeidan and Hannun, 2007). Many of the fundamental questions pertaining to the study of ceramide and sphingolipid-mediated cell regulation remain unresolved.

Sphingolipids are vectorially synthesized in the cell. The de novo biosynthesis begins with the condensation of serine and

R.P. Rao, T. Kosakowska-Cholody, and M.A. Masood contributed equally to this paper.

Correspondence to Jairaj K. Acharya: acharyaj@ncifcrf.gov

Abbreviations used in this paper: CERT, ceramide transfer protein; CPE, ceramide phosphoethanolamine; ERK, extracellular signal-regulated kinase; ES, embryonic stem; ESI, electrospray ionization; LC, liquid chromatography; MEF, mouse embryonic fibroblast; MS, mass spectrometry; PERK, protein kinase–like ER kinase; PDI, protein disulfide isomerase; SRM, single reaction monitor; TEM, transmission EM; UPR, unfolded protein response.

The Rockefeller University Press $30.00
J. Cell Biol. Vol. 184 No. 1 143–158
www.jcb.org/cgi/doi/10.1083/jcb.200807176

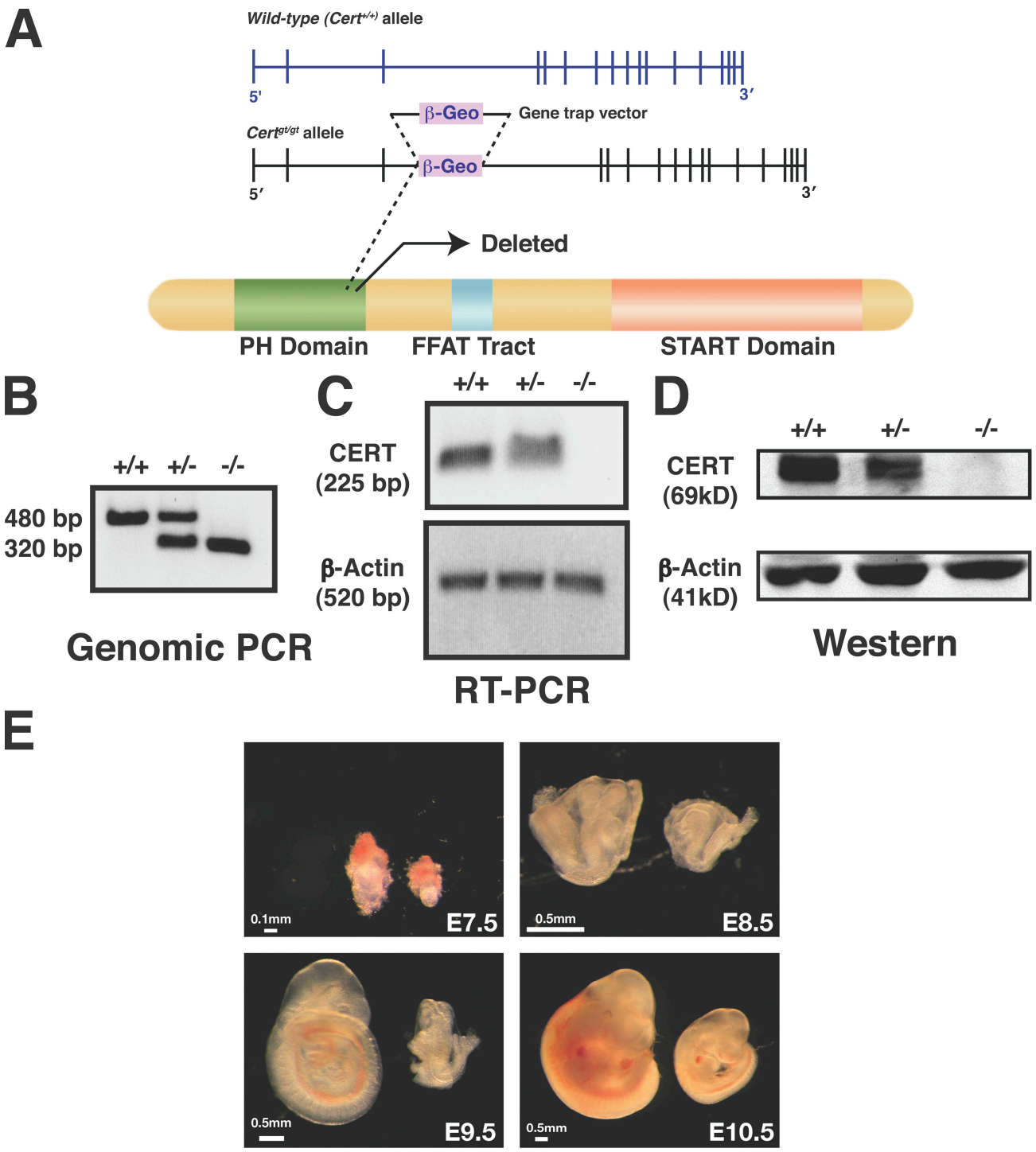

Figure 1. **Isolation of CERT-deficient (*Cert*$^{gt/gt}$) mice.** (A) The genomic organization of *Cert* is shown, and the location of the gene trap vector in the ES cell line RRF047 is depicted in the middle panel. This insertion results in truncation of the product within the pleckstrin homology (PH) domain of the CERT protein and results in a null or severely hypomorphic mutant. The insertion site was confirmed by sequence analysis of PCR products. The third intron of *Cert* is 26,177 bp long. The gene trap was inserted 18,394 nucleotides downstream of the 5′ end of this intron. START, steroidogenic acute regulatory protein related. (B–D) The genotype of the *Cert*$^{+/gt}$ heterozygous intercross was confirmed by genomic PCR across the insertion point (B), RT-PCR across exons 3 and 4 (C), and Western analysis (D) as described in Materials and methods. +/+, wild type; +/−, heterozygous mutant; −/−, homozygous mutant. (E) *Cert*$^{gt/gt}$ embryos have growth defects. The mutant embryos are smaller in size compared with wild type. These changes are obvious even in E7.5 embryos.

a fatty acyl Co-A; a series of reactions follow that leads to the generation of ceramide in the ER (Menaldino et al., 2003; Hanada, 2006). The subsequent steps of sphingolipid biosynthesis, including those of sphingomyelin and complex sphingolipids, require ceramide to be transported from the ER to the Golgi complex. Because ceramide is highly insoluble, an energy barrier impedes the movement of ceramide from one membrane to another, and cells accumulate pools of ceramide in different

Table I. **Genotypic analysis of offsprings from *Cert*$^{+/-}$ intercrosses**

Stage	Genotype			Absorption	Total
	+/+	+/−	−/−		
Newborn	195 (35%)	361 (65%)	0	NA	556
E7.5	5	8	4	NA	17
E8.5	11	19	10	NA	40
E9.5	26	32	12	NA	70
E10.5	25	44	22	5	91
E11.5	16	39	3	21	79
E12.5–14.5	11	21	0	9	41

NA, not applicable.

subcellular compartments. Recently, Hanada et al. (2003) demonstrated that CERT, a member of the signal transduction and activation of the RNA family of proteins, is responsible for the bulk of the ceramide transport from the ER to the Golgi complex. It localizes to the ER and the Golgi complex. CERT has three functional domains known to be involved in ceramide transport. An amino-terminal pleckstrin homology domain recognizes phosphatidylinositol 4-phosphate and targets CERT to the Golgi. An FFAT motif near the middle of the molecule is thought to interact with vesicle-associated membrane protein–associated protein to recruit CERT to the ER (Kawano et al., 2006). The C-terminal steroidogenic acute regulatory protein–related domain extracts ceramide from the ER membrane (Fig. 1 A; Hanada et al., 2003).

In this study, we evaluated the in vivo role of CERT in a mouse line lacking a functional *Cert* gene. We found that CERT is essential for embryonic survival, at least in part because of defects in proliferation and organogenesis with underlying ER and mitochondrial defects. Strikingly, this study also suggests that defects in the sphingolipid biosynthetic pathway that lead to ceramide accumulation can cause severe developmental disruption without inducing apoptosis.

Results

Generation of *Cert*$^{gt/gt}$ mice

The mouse *Cert* gene is on chromosome 13 and is encoded by 18 exons. The transcript has a short and a long form, with the short form containing 2,668 bp and the long form con taining 2,746 bp. The respective proteins contain 624 and 598 amino acids. To generate a mouse mutant of *Cert* (affecting both forms), we used the gene trap embryonic stem (ES) cell line RRF047 from BayGenomics (Stryke et al., 2003). We obtained the ES cell line and confirmed the insertion of the gene trap vector (pGT2Lxf) by RT-PCR and sequencing (Fig. 1 A). The vector carries a splice acceptor sequence upstream of a galactosidase reporter gene, *β-geo* (a fusion of β-galactosidase and neomycin phosphotransferase II). A PCR genotyping strategy differentiated the mutant and wild-type alleles from DNA extracted from embryos (Fig. 1 B). The deleted allele was null or severely hypomorphic because embryos homozygous for this allele, *Cert*$^{gt/gt}$ (labeled −/− in figures) embryos, did not generate full-length RNA as determined by RT-PCR, and there was little or no CERT detectable by Western analysis (Fig. 1, C and D). In contrast, CERT was clearly expressed in heterozygotes, *Cert*$^{+/gt}$ (+/−), although the amount was lower than in the wild type, *Cert*$^{+/+}$ (+/+). Because the expression of the inserted β-galactosidase gene is under the control of the endogenous *Cert* promoter, we expected β-galactosidase to be expressed in all of the tissues that normally express CERT. β-Galactosidase staining of embryonic day 9.5 (E9.5) embryos showed strong staining in homozygous mutant embryos, intermediate staining in heterozygotes, and none in wild-type embryos (Fig. S1 A, available at http://www.jcb.org/cgi/content/full/jcb.200807176/DC1). Sections through homozygous mutant embryos showed ubiquitous expression of CERT (Fig. S1 B), which was detectable between E8.5 and E10.5 by Western blotting (not depicted).

Cert$^{gt/gt}$ is an early embryonic lethal mutation

Genotypic analysis of >500 live-born progeny from heterozygote intercrosses revealed that 35% were wild type, 65% were heterozygous, and none were homozygous mutant (Table I), indicating that the *Cert*$^{gt/gt}$ mutation is a recessive embryonic lethal trait. Heterozygous mice, *Cert*$^{+/gt}$, were viable, fertile, and morphologically identical to wild-type *Cert*$^{+/+}$ littermates. To determine the developmental stage at which the *Cert*$^{gt/gt}$ fetuses die, embryos derived from *Cert*$^{+/gt}$ intercrosses were genotyped at different stages of gestation. We noticed several *Cert*$^{gt/gt}$ embryos degenerating and beginning to be absorbed at E11.5. Moreover, between E7.5 and E10.5, all three genotypes were present in the expected Mendelian ratio (1:2:1; although the size of the homozygotes appeared somewhat reduced throughout this time; Fig. 1 E and Table I). Therefore, we concluded that *Cert*$^{gt/gt}$ embryos die around E11.5.

We probed for molecular and cellular links between the observed defects and Cert's function. Therefore, we measured the sphingolipids in wild-type and mutant E10.5 embryos 24 h before the mutant embryos begin to die.

Sphingolipid metabolism is defective in *Cert*$^{gt/gt}$ mutant embryos

The sphingomyelin and ceramide levels in tissue extracts of E10.5 wild-type and mutant littermates were measured using nonpolar liquid chromatography (LC), electrospray ionization (ESI), and single reaction monitor (SRM) tandem mass spectrometry (MS) as described in Materials and methods (Han and

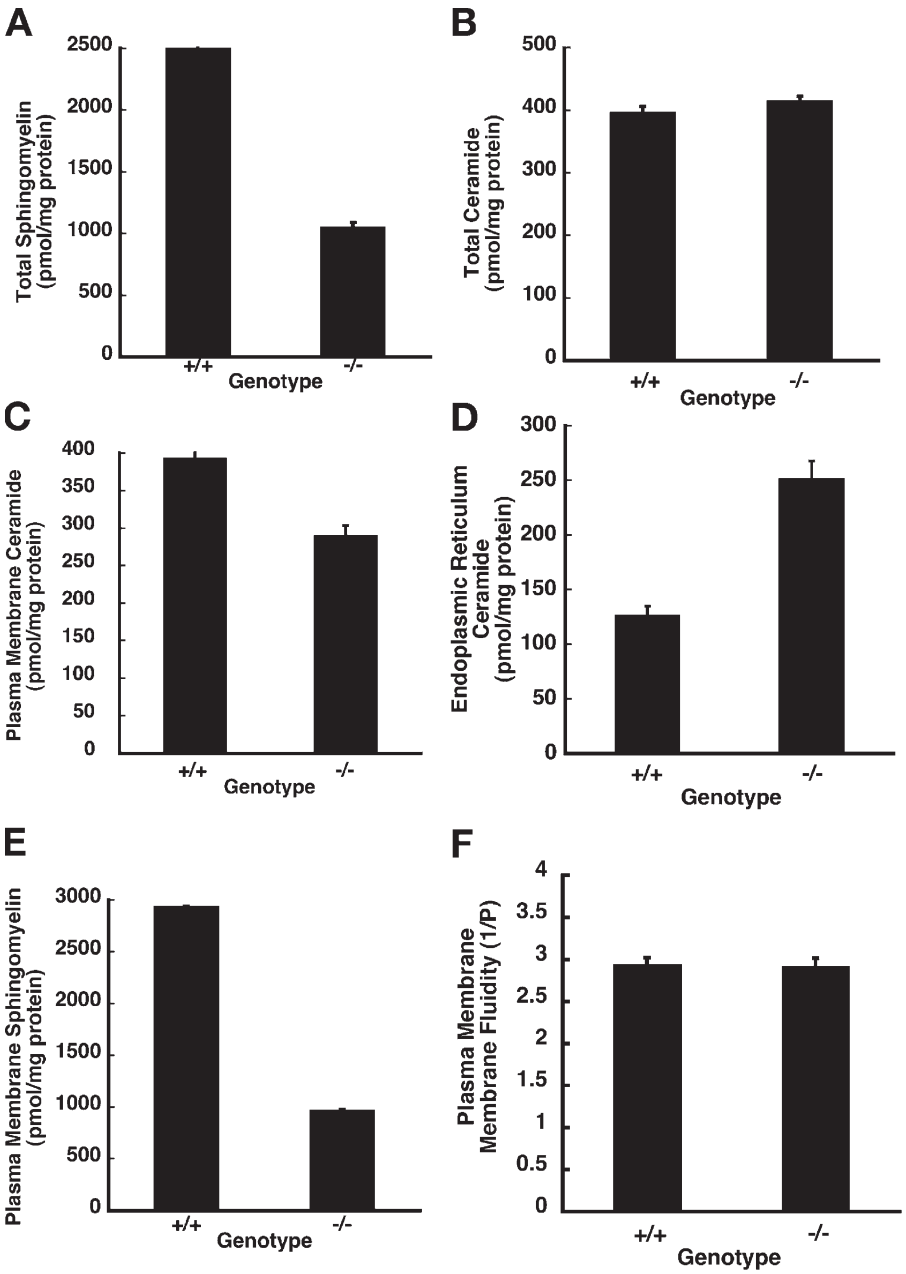

Figure 2. **Sphingolipid metabolism is disrupted in *Cert*$^{gt/gt}$ embryos.** The total cell and plasma membrane sphingomyelins and ceramides were estimated in E10.5 *Cert*$^{+/+}$ (+/+) and *Cert*$^{gt/gt}$ (−/−) embryos as described under Materials and methods. (A) The total sphingomyelin levels are decreased in mutant embryos. (B) The total cellular ceramides are indistinguishable between the mutant and the wild type. (C) The plasma membrane ceramides are decreased in the mutant embryos. (D) CERT deficiency and lack of ceramide transfer out of the ER cause increased ceramide levels by 200% in the ER. (E) The plasma membrane sphingomyelins are decreased by 52% in the CERT mutant embryos. (F) Plasma membranes were prepared by density gradient centrifugation using Opti-prep, and membrane fluidity was measured. No significant differences were found in the fluidity of plasma membrane between the wild type and the mutant. Error bars indicate standard deviation.

Gross, 2005; Merrill et al., 2005). The d-18 sphingolipids are the predominant species in mammals, and, therefore, we focused on the sphingomyelin and ceramides of this series. The total sphingomyelin level was ∼2,490 ± 55 pmol/mg of protein in the wild-type embryos but only 1,044 ± 45 pmol/mg of protein in the homozygous mutants, a decrease of ∼58% (Fig. 2 A). The breakdown of the individual species of the d-18:1 series from C-12 to C-26 is presented in Table S1 (available at http://www.jcb.org/cgi/content/full/jcb.200807176/DC1). Surprisingly, the total ceramides were not significantly different between the wild-type and mutant embryos (Fig. 2 B). The total ceramide levels for the d-18:1 series in wild-type embryos was 395 ± 11 pmol/mg of protein; in the mutant it was 413 ± 9 pmol/mg of protein. Because ceramide transport from the ER to the Golgi is compromised in the CERT mutants, the wild-type levels of total ceramide in the mutant could be explained if the ceramide level were lower than normal in the Golgi complex and the plasma membrane and higher than normal in the ER. Therefore, we measured the ceramide levels in these organelles from E10.5 wild-type and mutant embryos by MS. In the plasma membrane, the levels of ceramides were reduced in the mutant; the ER of the *Cert*$^{gt/gt}$ embryos had twice as much ceramide as in the ER of age-matched *Cert*$^{+/+}$ wild-type controls (Fig. 2, C and D; Fig. S1 C shows minimal contamination of ER by mitochondria and vice versa). The total hexosylceramide (glucosylceramides and galactosylceramides) content was lower in extracts of *Cert*$^{gt/gt}$ embryos compared with those of *Cert*$^{+/+}$ wild-type controls (Table S1).

A *Drosophila melanogaster* mutant lacking a functional CERT protein is defective in sphingolipid metabolism, and studies in mammalian tissue culture cells indicate that the biosynthesis of sphingomyelin is compromised when cells lacking CERT

are grown in serum-free media (Fukasawa et al., 1999; Rao et al., 2007). In *Drosophila* CERT-null mutants, both ceramide phosphoethanolamine (CPE; sphingomyelin analogue) and ceramide are decreased by >80%, and the decreased CPE in plasma membrane renders it more fluid and is responsible for the early death of these mutant flies. Because the plasma membrane sphingomyelin levels were decreased (Fig. 2 E) in the $Cert^{gt}/Cert^{gt}$ embryos, albeit not as much as in *Drosophila* CERT mutant ($dcert^{1}$) animals, we isolated and analyzed plasma membrane preparations from the $Cert^{+/+}$ and $Cert^{gt/gt}$ embryos. There were no significant differences in the fluidity of the plasma membrane between the wild-type and mutant cells (Fig. 2 F). The $dcert^{1}$ plasma membrane was used as the positive control (unpublished data). The decrease in sphingomyelin levels (58%) in $Cert^{gt/gt}$ mutant embryos is less than that observed in $dcert^{1}$ flies and might not be low enough to render the plasma membrane fluid.

Therefore, our data suggest that sphingomyelin-associated membrane fluidity was not contributing to the observed defects in the CERT-deficient mice. Thus, we investigated whether the accumulation of ceramide in the ER of $Cert^{gt/gt}$ embryos could affect its structure and function and thus compromise the viability of the cells.

ER and mitochondrial alterations in $Cert^{gt/gt}$ embryos

To evaluate whether the accumulation of ceramide affected the structure of the ER in the $Cert^{gt/gt}$ mutants, we examined sections from E8.5–10.5 embryos by transmission EM (TEM). Because the $Cert^{gt/gt}$ embryos exhibited cardiovascular defects (see section *$Cert^{gt/gt}$ mutants die around E11.5…*), we initially examined the hearts of E10.5 wild-type and mutant embryos. TEM analysis of cells from the endocardial, muscular, and epicardial regions showed proliferation, vesiculation, and even engorgement of the ER in the cells of the $Cert^{gt/gt}$ embryos (Fig. 3, top right). In many instances, these engorged ERs were accompanied by the accumulation of lipoid bodies in their vicinity (Fig. 3, bottom right, white arrow). Surprisingly, the mitochondria of $Cert^{gt/gt}$ cells were abnormal as well, appearing pale and engorged (Fig. 3, middle and bottom). Many lacked cristae; several were undergoing gross structural changes and degenerating.

If indeed the CERT deficiency was responsible for these changes and CERT function is ubiquitous, we expect to see similar structural changes in other cell types of the developing embryo. To address this, we examined the cells of the developing optic cup, an easily identifiable area of the developing embryo, by TEM. Mitochondrial changes similar to the ones seen in the heart were predominant in these optic cup cells in the mutant E10.5 embryos (Fig. S2, available at http://www.jcb.org/cgi/content/full/jcb.200807176/DC1). Although the ER and Golgi were the most visible structures in the wild-type $Cert^{+/+}$ cells, indicating healthy activity, the mitochondria in the mutant cells could be seen degenerating in the vicinity of lipid-filled structures.

To ascertain whether the compromised ER and mitochondria initiated the abnormal development of the CERT-deficient embryos, we also examined cardiovascular and optic cup cells from E9.5 embryos; that is, 48 h before the mutant embryos typically die. Although not as abundant as at E10.5, ER engorgement, vesiculation, and mitochondrial changes were visible in the E9.5 embryos in differentiating cells of both the optic cup and the heart, including the myocardial cells (Fig. S3, available at http://www.jcb.org/cgi/content/full/jcb.200807176/DC1).

Chronic ER stress in $Cert^{gt/gt}$ embryos

The morphological features of $Cert^{gt/gt}$ mutant cells are reminiscent of cells undergoing ER stress. ER stress manifests in cells as ER proliferation, dilation, and vesiculation (Scheuner and Kaufman, 2008). ER distension is a hallmark for cells that have defective protein folding in the ER lumen and is observed in response to the pharmacological induction of ER stress (Ermonval et al., 1997; Umebayashi et al., 1997; Scheuner et al., 2005). The ER is responsible for the synthesis of roughly a third of the proteins generated in a cell. Several hundred proteins, including those involved in lipid biosynthesis, are up-regulated when the unfolded protein response (UPR) signaling pathway is activated in yeast upon ER stress (Travers et al., 2000; van Anken and Braakman, 2005). It has become increasingly clear that components of the UPR are also up-regulated during development and differentiation in animals (Reimold et al., 2000; Bertolotti et al., 2001; Zhang et al., 2005). The defective transport of ceramide in vivo may therefore stress the ER and affect the viability of the cell and of the organism as a whole. Although it has been proposed that the accumulation of ceramide in the ER could cause stress, this has not been demonstrated experimentally.

We used Western blot analysis to compare the steady-state levels of a panel of proteins implicated in the ER stress response, i.e., BiP, protein disulfide isomerase (PDI), IRE1-α, protein kinase–like ER kinase (PERK), eIF2-α, and C/EBP homologous protein, in E10.5 $Cert^{+/+}$ and $Cert^{gt/gt}$ embryos (Fig. 4 A). IRE1, PERK, and ATF6 are considered the proximal sensors of the UPR signaling cascade (Malhotra and Kaufman, 2007; Ron and Walter, 2007). These proteins collectively monitor the quality of the proteins synthesized in the ER. Activation of these three proteins either in isolation or in concert when unfolded proteins accumulate in the ER or the ER is subjected to stress is thought to initiate a transcriptional and translational program. Acute or low-level chronic stress of the ER will initiate protective responses, and the cells adapt by regulating the induction of chaperones and modulating the capacity of the ER to synthesize and properly fold new proteins. However, severe or persistently toxic ER stress that cannot be resolved can activate components of the cell death pathway.

We found that phosphorylated PERK protein was slightly lower in the extracts of $Cert^{gt/gt}$ than in *Cert/Cert* mice (Fig. 4 A), and a proapoptotic downstream effector of phosphorylated PERK, C/EBP homologous protein, was unaffected (not depicted). IRE1-α levels were unchanged, and ATF6 was only slightly increased in the mutant embryos. However, some of the downstream components of the UPR pathway displayed significant changes: the protective ER chaperones calnexin, PDI, and ATF4 were increased in the $Cert^{gt/gt}$ cells (Fig. 4 B). In addition, phosphorylated eIF2-α, which is implicated in cell cycle arrest and attenuates the translation of general proteins

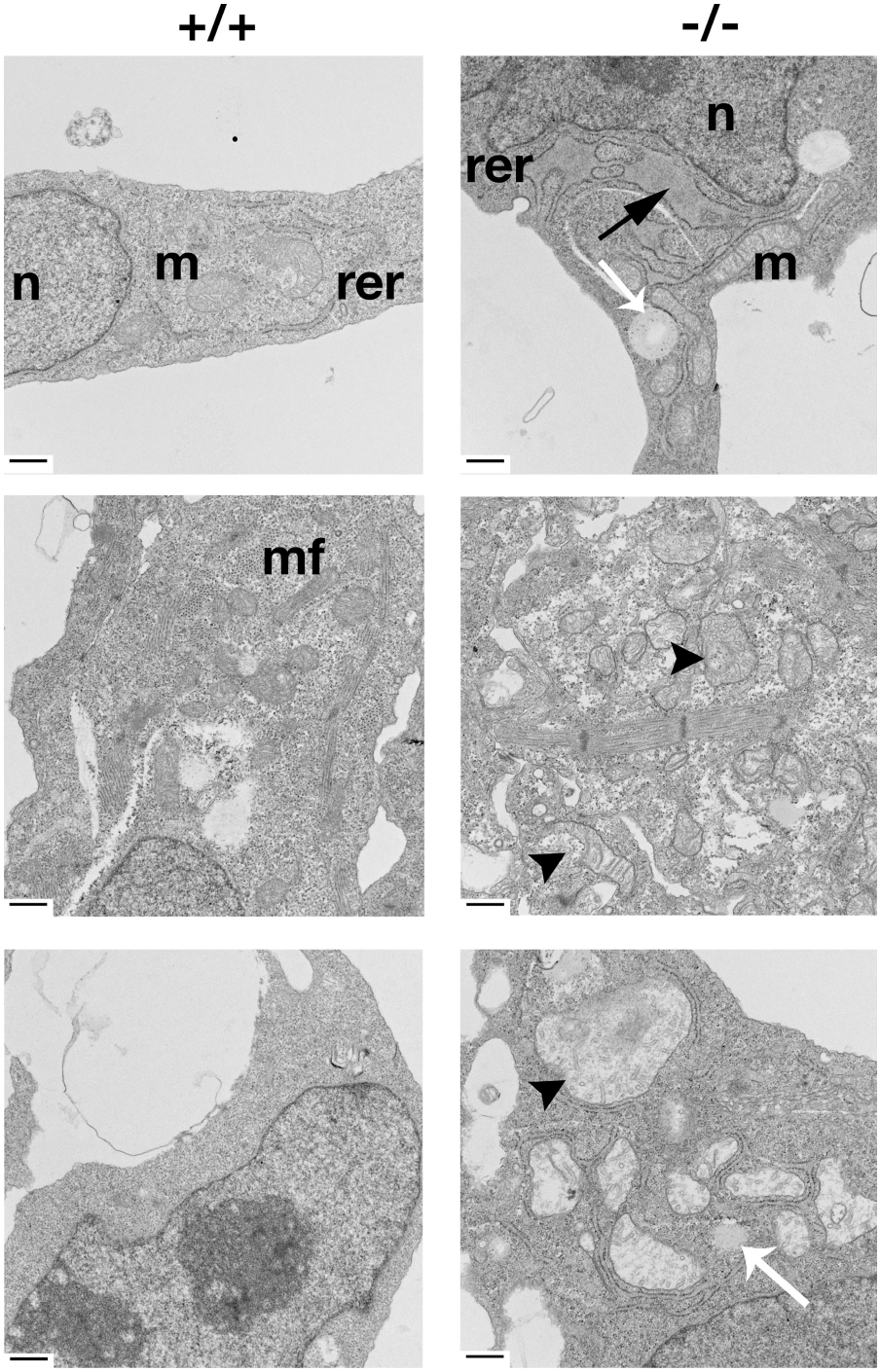

Figure 3. **EM evidence of ER and mitochondrial disorganization in *Cert*$^{gt/gt}$ embryos.** Cells from the three primary layers of the developing heart, namely endocardium, myocardium, and epicardium, of E10.5 *Cert*$^{+/+}$ and *Cert*$^{gt/gt}$ embryos were examined under an electron microscope. The panels on the left are from the *Cert*$^{+/+}$ (+/+) embryos, and the *Cert*$^{gt/gt}$ (−/−) mutants are on the right. The black arrow shows a lipid-laden engorged rough ER (rer) in the endocardial layer of the mutant heart. The white arrows show lipid-laden structures found in the vicinity of swollen ER and mitochondria (m) found often in the mutant cells. The arrowheads show mitochondria undergoing degeneration with discontinuous outer and inner mitochondrial membranes in the myocardial layer (middle). In the epicardial cells (bottom), the arrowheads depict swollen and pale mitochondria with ruptured inner and outer mitochondrial membranes in the mutant heart. The mitochondria in the mutant are generally swollen, pale, and have fewer cristae. n, nucleus; mf, muscle fibers of the myocardial cells. Bars, 500 nm.

under ER stress, leading to adaptation, was significantly upregulated in the *Cert*$^{gt/gt}$ embryos (Fig. 4 B). It is worth noting that the phosphorylation of eIF2-α has been reported to increase significantly during the G2/M phase in Ba/F3 cells and at the G2/M boundary in human osteosarcoma cells (Datta et al., 2005; Tinton et al., 2005). These observations suggest that *Cert*$^{gt/gt}$ embryos are undergoing a state of chronic ER stress. The biochemical evidence correlating the structural alterations with functional changes in the ER prompted us to probe whether a similar situation existed in the mitochondria of *Cert*$^{gt/gt}$ embryos.

Ceramide is increased in mitochondrial preparations of *Cert*$^{gt/gt}$ embryos

The accumulating ceramide causes ER stress, and the ceramide might be transferred to the mitochondria via recently discovered regions of close contact between the ER and mitochondria (Copeland and Dalton, 1959; Ruby et al., 1969; Morre et al., 1971; Meier et al., 1978; Eggens et al., 1979; Vance, 1991; Rizzuto et al., 2004; Franzini-Armstrong, 2007). Such a finding would show a strong correlation between the altered sphingolipid metabolism and the observed phenotypes in CERT mutant embryos. Therefore, we prepared mitochondrial preparations

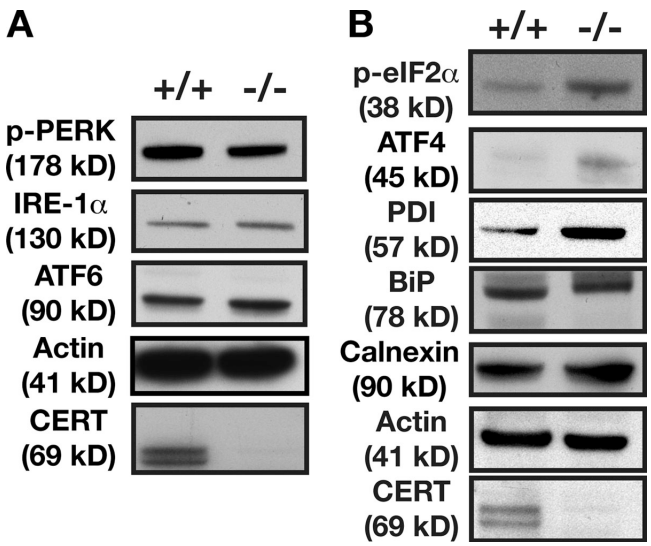

Figure 4. ***Cert*$^{gt/gt}$ embryos exhibit evidence of ER stress.** (A) Western blot analysis of cell extracts of E10.5 wild-type and *Cert*$^{gt/gt}$ embryos probed for proximal sensors such as phosphorylated PERK, IRE1-α, and ATF6 showing no or a slight increase in levels, a situation not different from cells in states of chronic stress. (B) Components of the UPR response implicated in the increased protein-folding efficiency of the ER such as ATF4, PDI, and calnexin were all increased in *Cert*$^{gt/gt}$ embryonic extract. The increased levels of phosphorylated eIF2-α are an indicator of the underlying ER stress. +/+, wild type; −/−, homozygous mutant.

from the wild-type *Cert*$^{+/+}$ and the mutant *Cert*$^{gt/gt}$ embryos and estimated ceramides in them. As shown in Fig. 5 A, the mitochondria of the mutants contained 1.5-fold more ceramide than those of the wild-type embryos. The lack of CERT function caused abnormal ceramide accumulation in the mitochondria of CERT-deficient embryos.

To determine whether mitochondrial functioning was compromised in the *Cert*$^{gt/gt}$ embryos, we evaluated the level of cytochrome *c* oxidase, the terminal enzyme of the oxidative phosphorylation cascade. Mitochondria were prepared using density gradient centrifugation, and the cytochrome *c* oxidase activity was measured. As shown in Fig. 5 B, the activity of cytochrome *c* oxidase was significantly lower in the mutant embryos than in wild-type embryos, indicating that the structural changes and lipoid degeneration observed in the CERT-deficient embryos resulted in compromised functioning of the mitochondria in these animals. Thus, the altered ceramide metabolism in the *Cert*$^{gt/gt}$ embryos not only affected the ER but also had a strong effect on mitochondrial integrity and function.

Cert$^{gt/gt}$ mutants die around E11.5 as a result of cardiovascular insufficiency

To correlate the underlying biochemical defects to the observed phenotype of the *Cert*$^{gt/gt}$ mutants, morphological assessment of embryos was performed. From the early head-fold stage (E7.5) to E10.5, the *Cert*$^{gt/gt}$ embryos were smaller than their wild-type *Cert*$^{+/+}$ counterparts (more the size of wild-type animals that were 0.5–1 d younger), although their gross appearance was similar to wild type (Fig. S1 A). To evaluate whether the growth defects began in early embryogenesis, we examined the outgrowth of *Cert*$^{gt/gt}$ blastocysts. E3.5 blastocysts were outgrown in ES media for 3 d, and no obvious developmental defect was found (Fig. S4, available at http://www.jcb.org/cgi/content/full/jcb.200807176/DC1). The inner cell mass and the outgrowth of the polyploid trophoectoderm cells in all three cultures were easily distinguished. We also followed cell proliferation in the blastocysts by incubating them with BrdU after 3 d of outgrowth. No significant differences were noted among the outgrowths of the three genotypes (unpublished data). Therefore, the changes leading to the observed size difference in *Cert*$^{gt/gt}$ mutants must manifest at a postimplantation stage.

CERT-deficient embryos obtained by caesarian section appeared normal at E8.5–10.5, although their growth was retarded. Gross examination of the mutant embryos at E10.5 did not reveal any major developmental defects, except in the heart. The heart is the first functional embryonic organ, one of the first to differentiate and begin to function in the developing mouse embryo around E10.5 (Sissman, 1970; Challice and Viragh, 1974). In all of the mutant embryos examined, the bilateral heart tubes had migrated between E8.5 and E9.0 to the midline and fused to form a single heart tube. Heartbeats were established in the E10.5 mutants, indicating that they were all developmentally past E9.5. Closer examination of the dissected heart revealed that all of the *Cert*$^{gt/gt}$ embryos displayed a normal S-shaped loop. However, the truncus arteriosus region of the outflow tract of some *Cert*$^{gt/gt}$ mutants (Fig. 6 A) was thin, transparent, and swollen, and the entire heart appeared swollen with thin and transparent walls in other embryos (Fig. 6, A and B, bottom right). In one embryo, the walls of the primitive ventricle displayed a region of higher density (Fig. 6 B, top).

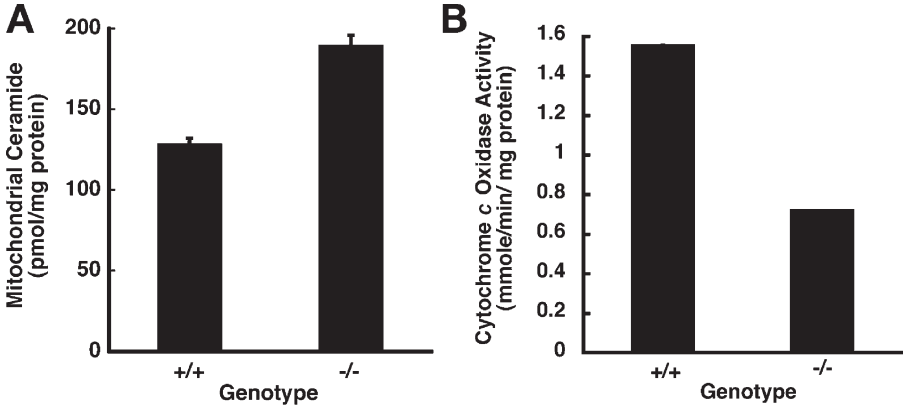

Figure 5. **Increased ceramide content in mitochondria of *Cert*$^{gt/gt}$ compromises mitochondrial function.** (A) CERT deficiency and lack of ceramide transfer out of the ER causes increased ceramide levels in the mitochondria. (B) The cytochrome *c* oxidase activity, the terminal reaction in ATP generation, was decreased by more than half in the mutant mitochondria (n = 3; error bars are very small and indicate the standard error of the mean). +/+, wild type; −/−, homozygous mutant.

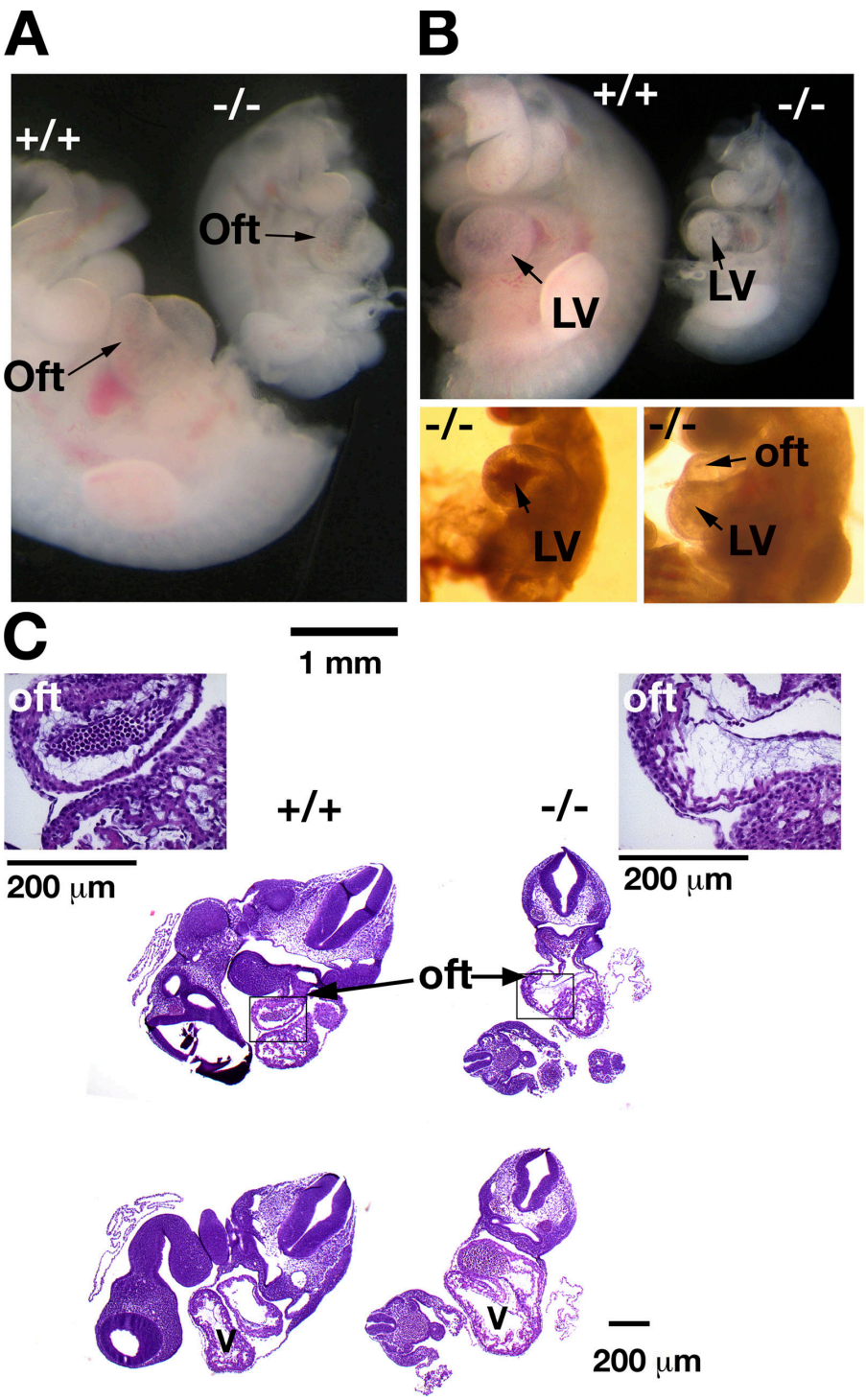

Figure 6. **Cardiac defects in *Cert*$^{gt/gt}$ embryos.** (A) Images of E10.5 *Cert*$^{+/+}$ (+/+) and *Cert*$^{gt/gt}$ (−/−) embryos. The heads were removed to facilitate the observation of the heart. In general, the mutant hearts were proportionately (relative to the size of the embryo) larger and thinner in the mutant compared with the wild type. (B, top) The same embryos in A were photographed from the other side to get a view of the left ventricle (LV), which, in this instance, appeared to have an area of increased density in the mutant embryo. The left bottom panel shows a mutant heart with accumulated blood in the left ventricle, and the panel on the right highlights the thin walls of the outflow tract (oft) and the left ventricle in the *Cert*$^{gt/gt}$ hearts. (C) H&E sections of the wild-type (+/+) and mutant (−/−) heart show the proportionately larger heart of the mutant with thin-walled ventricles and the outflow tracts. The inset shows a high magnification view of the outflow tract. In this instance, the mutant outflow tract is larger, thin walled, and increased the amount of the acellular cardiac jelly seen inside the cavity.

The contractions of the ventricles in the *Cert*$^{gt/gt}$ embryos were obviously weaker than in normal embryos, and blood accumulated in the ventricles of some animals (Fig. 6 B, bottom left).

Upon examination in utero, some *Cert*$^{gt/gt}$ embryos exhibited complete regurgitation of the blood into the heart during diastole, a phenomenon not observed in any of the wild-type or heterozygous embryos (Videos 1 and 2, available at http://www.jcb.org/cgi/content/full/jcb.200807176/DC1). Although in rare instances bradycardia and atypical contractions caused a partial backflow of blood in a few wild-type hearts during dissection and sample preparation at room temperature, we never observed in them the extreme regurgitation of blood observed in the mutant embryos. Furthermore, the mutant embryos were well past the 20-somite stage when embryonic hearts normally establish unidirectional blood flow.

Histological analysis revealed an enlarged ventricular cavity and thin walls (Fig. 6 C). Closer inspection showed that the outflow tract was enlarged and had thinner and weaker walls than the heterozygote or wild-type hearts, and the width of the acellular cardiac jelly between the inner endocardial cells and

the outer cardiomyocytes was also enlarged in many mutant hearts (Fig. 6 C, inset). In several mutant embryos, the ballooned and thin-walled heart chambers were so fragile that they were punctured during dissection, even with very gentle handling.

The combined gross and histological findings indicated that the *Cert*$^{gt/gt}$ embryos die around E11.5 from failure to establish a fully functional cardiovascular system. The nonproductive cardiac contractions indicated that there was a cardiac pump failure that caused venous dilation, which could lead to low blood pressure, systemic hypoxia, and eventual embryonic death.

Cell proliferation changes in *Cert*$^{gt/gt}$ embryos

At the cellular level, the growth defects of the *Cert*$^{gt/gt}$ embryos could arise either from aberrant proliferation and differentiation or excessive cell death. Thus, we evaluated the proliferative potential of *Cert*$^{gt/gt}$ embryonic cells by labeling dividing cells with BrdU (Fig. 7 A), which is incorporated during the S phase. The percentage of cells that incorporated BrdU was calculated in four different areas of each animal. The mutants had BrdU-positive indices that were significantly lower than those of wild-type *Cert*$^{+/+}$ embryos (Fig. 7 B). These results suggested that the cell cycle patterns of the *Cert*$^{gt/gt}$ embryos were aberrant, which could contribute to the observed defects in the growth and development of the mutant embryos.

To gain insight into the molecular changes affecting the cell cycle in the mutant embryos, we immunoblotted tissue extracts of E10.5 normal and mutant embryos for various cell cycle markers. As shown in Fig. 7 C, the levels of cyclin D1, a marker for G1 phase, and Cdc2, an essential cell cycle kinase and regulator of the G2/M transition, were decreased in the mutant embryos (Berthet and Kaldis, 2007; Satyanarayana et al., 2008). Moreover, the fraction of the inactive phosphorylated form of Cdc2 (Y15P-Cdc2) was higher in the mutant than in *Cert*$^{+/+}$ embryos, suggesting Cdc2 activity was lower in the *Cert*$^{gt/gt}$ embryos, a change that could delay the entry of cells into the G2/M phase.

Active Akt has been implicated in the regulation of cardiac myocytes and the proliferation of cardiac progenitor cells (Sussman, 2007). Therefore, we measured the Akt levels in the wild-type and mutant developing embryos. As shown in Fig. 7 D, we found that the level of phosphorylated Akt was down-regulated in the *Cert*$^{gt/gt}$ embryos, perhaps contributing, at least in part, to their decreased cell proliferation. Our findings show that the expression and regulation of key cell cycle proteins are affected in the mutant embryos, although further detailed studies will be required to understand the complexity of the deregulation. Furthermore, these results suggest that the *Cert*$^{gt/gt}$ proliferation deficiency occurs via a mechanism that is directly or indirectly linked to S- and M-phase entry.

Defects in *Cert*$^{gt/gt}$ embryos are not caused by increased apoptosis

The complex pathways involved in sphingolipid metabolism have been implicated in the regulation of apoptosis. To learn whether the excessive loss of tissue and the developmental defects of the *Cert*$^{gt/gt}$ embryos could be the result of apoptosis, cell death was measured by using TUNEL, as described in Materials and methods. As shown in Fig. 7 E, there was no difference in apoptotic cell death between mutant and wild-type embryos at E10.5, when all of the phenotypes described here were visible. The percentage of TUNEL-positive cells was determined by counting cells in at least six areas of each embryo and comparing results of corresponding areas in wild-type *Cert*$^{+/+}$ and mutant *Cert*$^{gt/gt}$ embryos. Our results indicated that the cellular and molecular events that precede and contribute to heart failure do not include abnormal apoptotic cell death. We also did not observe cellular changes consistent with increased apoptosis among cells of the developing heart and optic cup of *Cert*$^{gt/gt}$ embryo (unpublished data) while examining them for the aforementioned subcellular morphology.

Activation of MAPK survival pathways and the inactivation of Akt/PKB and JNK signaling in *Cert*$^{gt/gt}$ embryos

Our data suggested that the accumulation of ceramide caused by CERT deficiency led to the activation of ER stress and caused mitochondrial dysfunction. How do CERT-deficient cells cope with these defects and survive at E10.5? To profile the response of the CERT-deficient cells at the molecular level, we performed immunoblotting for a panel of proteins, phosphorylated and/or nonphosphorylated, that are implicated in stress-activated cell survival responses and apoptosis. MAPK and Akt/PKB signaling play critical roles in cell survival during stress. Therefore, we evaluated the steady-state levels of these proteins in wild-type and mutant embryos by Western blotting. Surprisingly, the levels of the phosphorylated form of Akt were down-regulated in the mutant extracts compared with total Akt (Fig. 7 D).

Although the difference in phosphorylated Akt could partly account for the cell cycle arrest/delay observed in CERT mutant cells, it could not fully explain the ability of the mutant cells to survive the ER stress. Therefore, we investigated the MAPK cell survival pathways. The MAPK signaling cascades are involved in stress-activated signaling responses. Extracellular signal-regulated kinase (ERK), JNK, and p38 MAPK are subgroups of the MAPK family. The dynamic balance between the activated ERK– and JNK–p38 signaling pathways is important in determining cell survival versus apoptosis. As shown in Fig. 8 A, the ERK survival pathway was significantly activated in the mutants, but the JNK–p38 pathway was down-regulated. Therefore, cellular survival under ER stress in *Cert*$^{gt/gt}$ embryos involves a mechanism in which the ERK pathway is activated and the Akt, JNK, and p38 signaling pathways are suppressed.

A notable feature of the UPR is that it leads to the concomitant engagement of both adaptive and proapoptotic molecules. Thus, we extended our analysis to see whether such a phenomenon had been initiated in the *Cert*$^{gt/gt}$ mice. We immunoblotted extracts from E10.5 embryos to look for the possible activation of cell death pathways (Fig. 8 B). Surprisingly, the proapoptotic proteins Bax and Bak were significantly elevated in the *Cert*$^{gt/gt}$ embryos, and the antiapoptotic Bcl-2 and Bcl-x_L were down-regulated. It is worth noting that the Bcl-2 family proteins also play important roles in ER physiology and regulate

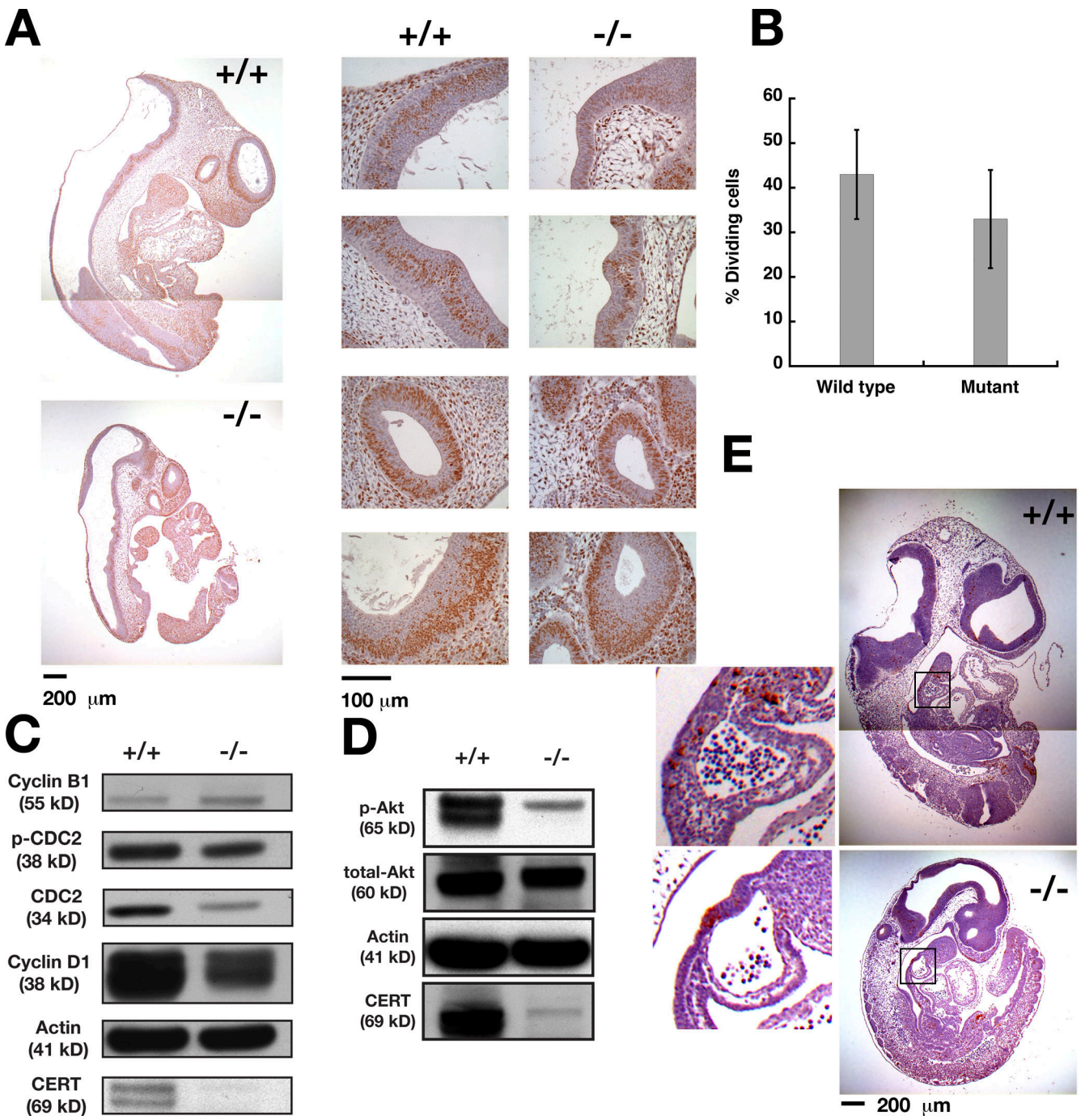

Figure 7. **Growth and cell cycle defects without increased apoptosis in *Cert*$^{gt/gt}$ mutant embryos.** (A) Pregnant mice were injected with BrdU 1 h before dissection, and E10.5 embryos were dissected, genotyped, and stained for BrdU uptake as described in Materials and methods. Four of the areas chosen for counting the fraction of dividing cells are shown in the panels to the right. (B) *Cert*$^{gt/gt}$ embryos showed a lower fraction of BrdU-positive cells, indicating a slower rate of cell division in these mutant embryos. Error bars indicate standard deviation; $n = 4$. (C) Western blot analysis for some of the components of the cell cycle in *Cert*$^{+/+}$ (+/+) and *Cert*$^{gt/gt}$ (−/−) embryos. (D) Phosphorylated Akt levels are decreased in *Cert*$^{gt/gt}$ embryos. (E) TUNEL staining of E10.5 wild-type and mutant embryos. Insets show boxed areas at higher magnification. There were no significant differences in the proportion of dying cells between the wild-type and mutant embryos. Note that the wild-type embryos are large compared with the mutant and, therefore, were photographed twice to include the upper and the lower halves of the embryo. The composites are shown in A and E.

mitochondrial morphogenesis (Karbowski et al., 2006). Bax and Bak were recently shown to act not only as essential gateway proteins to cell death pathways operating at the mitochondria but also to relocate to the ER to function in the regulation of UPR (Wei et al., 2001; Hetz et al., 2006; Oakes et al., 2006). Bax accumulated in postmitochondrial supernatant rather than in the mitochondria (Fig. 8 C), supporting a nonmitochondrial role for the increased Bax protein. Also, the total level of cytochrome *c*, a key molecule released from mitochondria into the cytosol in the mitochondrial apoptotic pathways, was clearly decreased in the *Cert*$^{gt/gt}$ embryos. In contrast, the level of apoptosis-induced factor was not affected (Fig. 8 C). Because the

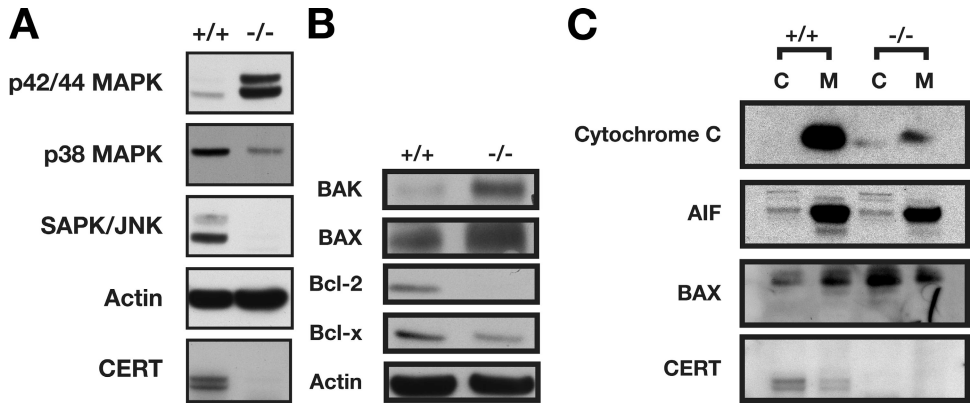

Figure 8. **Cell survival pathways are activated in E10.5 *Cert*$^{gt/gt}$ embryos.** (A) Components of the cell survival pathway p42/44 ERK are strongly activated in the mutant, whereas MAPK components that mediate stress-mediated response are suppressed. SAPK, stress-activated protein kinase. (B) Components of the apoptotic machinery such as Bak and Bax that also have roles in mediating UPR are activated, whereas antiapoptotic components Bcl-2 and Bcl-x are down-regulated. (C) The total cytochrome *c* levels in *Cert*$^{gt/gt}$ embryos are decreased significantly in the mutant embryos. Although most of the cytochrome *c* is in the mitochondria in the wild type, in the mutant we see it in both cytosol (C) and mitochondria (M). Also, the increased Bax in *Cert*$^{gt/gt}$ embryos is in the cytosol, whereas mitochondrial levels seem unaffected. AIF, apoptosis-induced factor.

Cert$^{gt/gt}$ embryos showed no sign of apoptosis, it was clear that several factors influenced the survival of the CERT-deficient cells, although the compensation was not vigorous enough to overcome the growth delays imposed on cells under chronic ER stress (Rutkowski et al., 2006).

Our data suggested that although activators of apoptosis were initiated in the CERT-deficient cells, the effectors were not deployed to execute apoptosis. One reason for the lack of deployment could be the low level of cytochrome *c* in the mutant embryos. In addition, the predominant activation of proteins in the cell survival pathways of the MAPKs could contribute to this effect. We have also confirmed that CERT deficiency does not inherently compromise the apoptotic potential of the mutant cells. Primary mouse embryonic fibroblasts (MEFs) can be derived and cultured from the mutant E9.5 embryos. Although they are slightly growth inhibited compared with similarly derived wild-type MEFs, they are capable of undergoing actinomycin D–induced apoptosis ex vivo (Fig. S5, available at http://www.jcb.org/cgi/content/full/jcb.200807176/DC1). A very high ADP/ATP charge ratio, an indicator of the inability to undergo apoptosis, was also not a contributing factor in the mutant embryos because these ratios were similar in the wild-type and the mutant embryos. Also, total ATP levels were comparable between the wild-type and mutant embryonic extracts, implying that insufficient ATP was not responsible for the failure to undergo apoptosis (unpublished data).

Discussion

In this study, we showed that CERT, a protein that transports ceramide from the ER to the Golgi, is essential for survival in mice. Mice lacking CERT die at E11.5 because of cardiac abnormalities manifesting as a result of underlying structural and functional defects in ER and mitochondria. The in vivo significance of ceramide transfer from the ER to the Golgi was studied recently using a *Drosophila* model (Rao et al., 2007). Flies lacking a functional CERT protein are viable and fertile but die prematurely as a result of accelerated aging. The different outcomes in these organisms stem not only from the differences in their developmental programs but also from differences in the underlying biochemical changes accompanying the CERT deficiency.

CERT mutants in both organisms have decreased sphingomyelin levels (CPE in *Drosophila*). Although there is a fourfold decrease in the *Drosophila* adult, there is slightly more than a twofold decrease in the mutant mouse embryos. This is probably because the mouse embryos, unlike *Drosophila*, developed within the uterus of a heterozygous mother, where sphingomyelin, a component of plasma lipoprotein fraction, can be delivered to the developing embryos through the amniotic fluid (Liu et al., 1992; Subbaiah and Liu, 1993). In an analogous situation, CERT-deficient CHO cells (Ly-A), when grown in the presence of serum, do not show changes in steady-state sphingomyelin levels because they can incorporate the metabolites from the medium (Fukasawa et al., 1999; Hanada et al., 2003). However, experimental evidence for this explanation of the differences in sphingomyelin levels is lacking. In any case, the effects of the decrease differ in mice and *Drosophila*: the very significant decrease in the CPE levels of *Drosophila* CERT mutants affects plasma membrane fluidity and initiates oxidative stress; the smaller decrease in sphingomyelin in the CERT-deficient mouse embryo did not alter plasma membrane fluidity. In *Drosophila*, total ceramide levels decrease by 80%, whereas they remain unchanged in mice. However, in the mouse embryo, a 200% increase in ceramide levels in the ER instigates a series of pathophysiological changes and ultimately causes early embryonic lethality.

The most important finding of this study is the impact of deficient ceramide transport on mitochondrial structure and function in mice. Mass spectrometric data indicated increased levels of ceramide in the mitochondria and ER, and electron micrographic pictures showed progressive degeneration of the mitochondria. The changes in ceramide levels and in the structure and function of mitochondria that accompany the CERT deficiency in mice support the idea that ceramide is normally directly transferred from the ER to the mitochondria. Studies have demonstrated a close functional link between the ER and

mitochondrial physiology (Copeland and Dalton, 1959; Ruby et al., 1969; Morre et al., 1971; Meier et al., 1978; Eggens et al., 1979; Vance, 1991; Rizzuto et al., 2004; Franzini-Armstrong, 2007). Several of these studies have even demonstrated a physical link between the ER and mitochondria. ER membranes called mitochondria-associated membranes are physically and functionally allied with mitochondria and have been implicated in the integration of several aspects of ER and mitochondrial function. Mitochondria-associated membranes are also involved in multiple mechanisms of the cooperative synthesis by the two organelles of the mitochondrial cytochrome *c* oxidase and phospho- and glycerosphingolipids (Shore and Tata, 1977; Vance, 1991; van Meer and Lisman, 2002). A recent electron tomography study demonstrated the existence of 10-nm and 25-nm tethers connecting smooth and rough ER, respectively, to mitochondria (Csordas et al., 2006). Furthermore, although sphingolipid levels are low in mitochondria, some enzymes involved in the de novo steps of the sphingolipid biosynthetic pathway, including ceramide synthase and ceramidase, have been reported to localize to mitochondria (Bionda et al., 2004). Our data support the idea that some mechanism exists for the transfer of ceramide from the ER to the mitochondria, either by physical continuity between the organelles or by a transfer protein. Although delivering sphingolipid metabolites to the mitochondria may serve a useful function in healthy cells, it might also serve to mitigate the effect of the sphingolipids accumulating in the ER during stressful or pathological conditions.

In a recent study probing the mechanism of drug resistance in tumor cells, it was shown that down-regulation of CERT sensitized these cells to the cytotoxic effects of paclitaxel and potentiated paclitaxel-induced ER stress (Swanton et al., 2007). However, in this study, we demonstrate that under physiological conditions, in vivo loss of CERT induces a state of chronic stress in the ER and, most importantly, compromises mitochondrial structure and function. The state of chronic stress in CERT mutant embryos is comparable with that of cells that are exposed to chronic ER stress but that have adapted to the stress. In a study of different states of ER stress, cells exposed to low concentrations of tunicamycin showed UPR activation and ER perturbation, but the cells still proliferated, although at a slower rate than untreated cells, and did not show any signs of apoptosis (Rutkowski et al., 2006). The chronically stressed cells achieved confluence and could be passaged for as long as their untreated counterparts (and they eventually achieved a near-normal growth rate) despite the continued presence of tunicamycin in the culture. Thus, the decreased proliferation of the tunicamycin-treated cells was caused by a growth delay, and chronic ER stress by exogenous pharmacological manipulation does not necessarily result in cell death, although death could be caused by a secondary mitigating event. Similarly, physiological activation of the UPR is observed in B lymphocytes as a result of increased demands of protein secretion (Wu and Kaufman, 2006).

The lack of CERT function in mice did not result in cell death. The biochemical data suggest that the cells mounted an adaptation response to the ER and mitochondrial stress in the mutant embryos. Because CERT performs a fundamental function in sphingolipid metabolism, it is present in all cells and tissues. Perhaps surprisingly, although none of the cells in the $Cert^{gt/gt}$ mice could transport ceramide, they could still divide at a compromised rate, and they progressed through a nearly normal developmental program until about E10–11.5.

This stage is a remarkable period in mouse development. Beginning around E8 and lasting until around E11.5, there is a sudden increase in the growth and complexity of the embryo (Viragh and Challice, 1973). The sudden shift in the pace of division and differentiation imposed on the CERT mutant cells at these stages apparently outstrips the ability of these compromised cells to respond to developmental signals. This notion is partly supported by our EM data that showed at E9.5 the beginnings of changes to the mitochondria and ER that were much more obvious at E10.5. That the animals died of cardiovascular defects is very reasonable in this context. During the 24-h window between E8.0 and E9.0, the linear dimensions of the heart increase four- to fivefold, which apparently pushed the mutant cells beyond their capacity to adapt. Because a functional circulatory system is an early requirement for survival and growth, its developmental failure resulted in early death attributable to the lack of CERT function. However, the underlying pathology existed in all of the embryonic cells, as indicated by the similar mitochondrial and ER changes observed in the cells of the developing eye.

Our study clearly demonstrates that manipulation of sphingolipid flux in vivo and the consequent accumulation of ceramide within cellular compartments do not necessarily end in apoptotic cell death. In the present study, it leads to defects in cell cycle and differentiation caused by the stress imposed on the ER and mitochondria. In sum, our combined approach has identified the essential role of CERT in mammalian embryogenesis and provided molecular insight into the role of the de novo sphingolipid biosynthetic pathway in influencing the ER-dependent structure/function of mitochondria.

Materials and methods

Generation of CERT knockout mice

The BayGenomics mouse (strain 129/Ola) ES cell line RRF047 was obtained and confirmed by RT-PCR. The gene trap vector (pGT2Lxf) was inserted in the *Cert* gene between exons 3 and 4 (26 kb). These cells were injected into C57BL/6 blastocysts, which were then implanted into pseudopregnant foster mothers. High-contribution chimeras were obtained. Heterozygous mice were backcrossed to C57BL/6 mice and kept in a 129/Ola cross C57BL/6 background. Therefore, all of the following experiments were performed with mice of the mixed genetic background. All mice were held in accordance with institutional policies and federal guidelines.

Mice were genotyped by a three-primer PCR using mouse tail DNA as a template. The primer sequences used were as follows: forward, 5′-CTCATGATCATCGTGGTAGAGAGAC-3′; mutant reverse, 5′-CCTACATAGTTGGCAGTGTTTGGGG-3′; and wild-type reverse, 5′-GTATGTTCAGGTAACTGTGGAGGC-3′. These primers amplified bands of 319 bp and 481 bp for the mutant and wild-type allele, respectively. PCR reactions began with a denaturing step at 95°C for 3 min followed by 35 cycles of 95°C for 30 s, 55°C for 30 s, and 72°C for 30 s.

Embryo dissection and histological and EM analyses

Timed mating was performed with $Cert^{+/gt}$ (+/−) mice on a mixed genetic background (C57BL/J129). Females with copulation plugs were considered to be at day 0.5 of gestation, and embryos present in this pregnant female were designated at E0.5. Pregnant females were dissected at various times of gestation, and the dissected embryos were photographed under a normal inverted light microscope (Axioskop; Carl Zeiss, Inc.)

connected to a digital camera (Powershot S50; Canon), and DNA for genotyping was isolated from small pieces of yolk sac by hot-start PCR lysis buffer (25 mM NaOH and 0.2 mM EDTA) and neutralization buffer (40 mM Tris-HCl). Genotyping was performed by the aforementioned 3 primer hot short PCR. For histological analysis, embryos were fixed with 4% paraformaldehyde (HCHO), embedded in paraffin, sectioned, and stained with hematoxylin and eosin (H&E). Photomicrographs were taken using a microscope (Axiophot; Carl Zeiss, Inc.) and a digital camera (CoolSNAP HQ; Photometrics). For EM analysis, embryos were fixed in 4% HCHO and 2% glutaraldehyde in 0.1 M sodium cacodylate buffer and processed as described previously (Acharya et al., 2006). Serial sections were viewed on an electron microscope (EM300; Philips Electronic Instruments, Inc.).

For blastocyst outgrowths, heterozygous 4–6-wk-old female mice were superovulated by intraperitoneal injection of a pregnant mare's serum (5 IU per animal) and human chorionic gonadotropin (5 IU per animal) 48 h later and were subsequently mated with *Cert*$^{+/gt}$ (+/−) males. Plugged females were killed, and their uteri were dissected and flushed with ES cell medium at 3.5 d after coitus. Single blastocysts were seeded onto gelatinized 96-well plates containing 200 µl of medium and incubated at 37°C and 5% CO_2. After 3 d, wash by PBS and blastocyst DNA was isolated by lysis buffer with proteinase K. The 3 primer PCR was performed.

LacZ staining was performed on E9.5 embryos dissected from the intercross of *Cert*$^{+/gt}$ in PBS, and embryos were transferred to 4% HCHO in PBS at 4°C and incubated in the dark for 1 h. Embryos were washed with rinse buffer (5 mM EGTA, 0.01% deoxycholate, 0.02% NP-40, and 2 mM $MgCl_2$ in PBS) at room temperature three times for 15 min. The embryos were incubated in the dark with freshly prepared staining buffer (5 mM $K_3Fe[CN]_6$, 5 mM $K_4Fe[CN]_6$, 5 mM EGTA, 0.01% deoxycholate, 0.02% NP-40, 2 mM $MgC1_2$, and 1 mg/ml X-gal solution in PBS) at 37°C overnight. Tissue sections were rinsed and stored in PBS and observed under a dissection microscope (Stemi DV4; Carl Zeiss, Inc.).

For BrdU, TUNEL staining, and immunohistochemistry, pregnant mice at E10.5 were injected intraperitoneally with BrdU (100 mg/kilogram of body weight; Sigma-Aldrich) 1 h before the embryos were collected. Embryos were isolated and fixed in 10% formalin solution (neutral buffered; Sigma-Aldrich) and 70% ethanol, respectively, before histological processing. Sagittal or transverse sectioning of samples embedded in optimal cutting temperature medium (Sakura Finetek) and immunohistochemistry staining of the tissues or organs of the embryos were performed by the Pathology/Histotechnology Laboratory at the National Cancer Institute at Frederick. In brief, transverse and sagittal heart sections were stained with H&E. Embryo sections were stained with ApopTag kit (Millipore) for apoptosis or antibodies against BrdU (Invitrogen) for proliferation according to the manufacturer's instructions. The slides were examined with a 5×, 20×, or 40× lens (bright field) under a microscope (Axioplan 2; Carl Zeiss, Inc.).

Subcellular fractionation for sphingolipid analysis and membrane fluidity measurement

Plasma membrane was isolated by density gradient centrifugation, and membrane fluidity was measured as described previously (Eroglu et al., 2003; Rao et al., 2007). Embryos were washed thoroughly in PBS containing 0.5% Triton X-100 and were homogenized in homogenization buffer (100 mM Tris-HCl, pH 7.4, 150 mM sodium chloride, and 0.2 mM EGTA with protease inhibitor mixture). The homogenate was centrifuged at 1,000 *g* for 10 min to get rid of cell debris. The resulting postnuclear supernatant was mixed 1:2 with Opti-prep, resulting in a 40% solution. 30 and 5% Opti-prep solutions were overlaid on the top. The tubes were centrifuged for 3 h at 100,000 *g*. Plasma membrane appeared as a white dense band at 30–5% interface.

Mitochondria and ER were isolated by following previously published protocols with some modifications (Bozidis et al., 2007). In brief, the embryos were homogenized in homogenization buffer A (20 mM Na-Hepes, 0.1 mM EDTA, and 0.2 M sucrose) with protease inhibitors. The homogenate was centrifuged at 1,000 *g* for 10 min, and the resulting supernatant-I was carefully aspirated into a new tube and centrifuged at 12,000 *g* for 15 min. The pellet enriched in mitochondria was washed twice with the aforementioned buffer and used for cytochrome *c* oxidase assay. The supernatant-II (postmitochondrial supernatant) was centrifuged at 150,000 *g* for 2 h, and the pellet was suspended in Hepes-EDTA buffer (20 mM Hepes and 0.1 mM EDTA) and loaded on top of the sucrose gradient tube (discontinuous gradient made with 2-, 1.5-, and 1.3-M sucrose solutions in Hepes-EDTA buffer). The contents were centrifuged at 152,000 *g* for 70 min. The ER that appears as a band at the interface of the 1.3-M sucrose gradient was collected into a new tube. The admixing of ER and mitochondrial fractions were monitored by evaluating the ER resident protein BiP and mitochondrial marker protein Grp 75 in the preparations. There was <5% mixing of mitochondrial resident protein Grp 75 in ER preparation and, likewise, <1% of ER protein BiP in mitochondrial preparation (Fig. S1 C).

Sphingolipid standards were purchased from Sigma-Aldrich and Avanti Polar Lipids, Inc. The ceramide/sphingolipid internal standard mixture (LM6002), which contains a mixture of 10 sphingolipids, each present at a concentration of 25 µM, was purchased from Avanti Polar Lipids, Inc.

Primary MEF culture and cell death analysis

E9.5 embryos were separated from the yolk sac, washed twice with PBS, pH 7.2, and trypsinized for 10 min. The cells were disaggregated by pipetting several times and suspended in 1 ml of prewarmed (37°C) DMEM supplemented with 10% FBS. The suspension was allowed to stand for 2–3 min at room temperature, and visible clumps were removed. The suspension was further centrifuged at 500 *g* for 3 min, and the cell pellet was suspended in MEF media (DMEM + 10% FBS) and plated on a 48-well plate. The plates were incubated at 37°C with 3% oxygen and 5% carbon dioxide as described previously (Parrinello et al., 2003). The medium was replaced the next day, and the cells were cultured for 4–5 d. For induction of apoptosis, the cells were treated with 10 µM actinomycin D for 12 h, after which the cell death was assessed using Vybrant apoptosis assay kit #2 (Invitrogen) according to the manufacturer's instructions. The images were obtained on a microscope (Axioplan 2) at a magnification of 40 using Axiovision 4.2 (Carl Zeiss, Inc.) and pseudocolored using Photoshop (Adobe). For tabulation reported in Fig. S5, 68–218 cells were counted from three separate primary MEFs derived from *Cert*$^{+/+}$ E9.5 embryos, and between 52 and 157 cells were counted for three primary MEF lines derived from E9.5 *Cert*$^{gt/gt}$ embryos.

Sphingolipid estimation

Preparation of lipid extracts from tissues. Lipid extracts were prepared, and sphingolipids were estimated according to the method described previously (Han and Gross, 2005; Merrill et al., 2005). In brief, to each of the 50–100 µl of sample having a protein concentration of ∼3–4 mg/ml, 0.5 ml CH_3OH, 0.25 ml $CHCl_3$, 50–100 µl of water, and 30 µl of a 25-µM solution of LM6002 internal standard were added. The lipid aggregates in the mixture were dispersed by either sonicating four times using a tip sonicator (Branson) at an amplitude of 30% for a period of 10 s or using a water bath sonicator for ∼15–30 min. After sonication, the samples were incubated overnight at 48°C with shaking. After cooling, 75 µl of 1-M methanolic KOH solution was added to each of the tubes followed by incubation at 37°C for 2 h with shaking. Each of the samples was then divided into two equal aliquots.

One of the aliquots was evaporated to a volume of ∼25 µl using a Speed Vac Concentrator (Savant Instruments, Inc.) and reconstituted with 300–400 µl of 1:1 (vol/vol) reverse phase solution A and reverse phase solution B. After vortexing for 1 min and centrifugation, the supernatant was collected.

The other aliquot was neutralized by an addition of 3–4 µl CH_3COOH followed by the addition of 2 ml of water and 1 ml $CHCl_3$. The biphasic solution was vortexed for 1 min, and the lower organic phase was collected. This extraction procedure was repeated once more. The combined organic fractions were evaporated using a heating block set at 50°C. Samples were reconstituted in 300–400 µl of 1:4 (vol/vol) $CHCl_3$–nonpolar mobile phase solution A. Ceramides and sphingomyelins were analyzed from this solution by normal phase LC-MS.

Quantitation of ceramide and sphingomyelin molecular species by LC electrospray tandem MS. LC-MS analyses were performed using a mass spectrometer (LTQ Discovery LC-MS; Thermo Electron Corp.) consisting of a Quantum triple stage quadrupole mass spectrometer equipped with an ESI source. The mass spectrometer was coupled to a high-performance LC system (1100 series; Agilent Technologies).

Complex sphingolipids (such as ceramides and sphingomyelins) were separated by normal phase high-performance LC using a binary system and a Supelcosil LC-NH_2 column (internal diameter = 3.0 mm, length = 7 cm, and mean particle size of the medium = 3 µm) operating at a flow rate of 250 µl/min. The column was maintained at 37°C. Mobile phase A consisted of 20 ml MeOH, 5 mM NH_4OAc, 15 ml CH_3COOH, 270 ml MeCN, 295 ml EtOAc, and 400 ml hexanes. Mobile phase B consisted of 99:1 (vol/vol) CH_3OH-CH_3COOH containing 5 mM NH_4OAc. The LC gradient run time for the analyses of ceramides and sphingomyelins was either 17 or 21 min.

The mass spectrometer (TSQ Quantum Discovery; Thermo Electron Corp.) was calibrated using a solution of polytyrosine-1,3,6 as recommended by the manufacturer. The tune file for ceramides, sphingomyelins, etc. was obtained by optimizing ESI source conditions at an LC flow rate of 250 µl/min and using ceramide and sphingomyelin reference compounds. The optimized source parameters used were as follows: sheath gas pressure, 20 psi; auxiliary gas pressure, 3 (arbitrary units); ion spray needle voltage, 4,500 V; capillary temperature, 377°C; skimmer offset, 5 V. No source fragmentation was observed when direct infusion of reference compounds was made at this skimmer potential, thus ensuring that maximum sensitivity is obtained. For sphingomyelin, the collision energy and tube lens values were obtained through compound optimization. For ceramides, tuned values for the tube lens were used, and application of universal 28–30 V of continuous extraction gave the best $[M+H]^+ \rightarrow$ 264 or 266 product ion fragments for all of the ceramides.

Nitrogen gas was used for collisionally induced dissociations in Q2, which was offset from Q1 by 10 V. SRM scans were acquired by setting Q1 and Q3 to pass the precursor $[M+H]^+$ and product ions 184 for sphingomyelin and 264 or 266 for ceramides containing sphingosine and sphinganine, respectively. The acquisition parameters common to all analytes were scan width (mass/charge ratio), 0.050 D; scan time, 0.10 s for each transition; peak width (full width half maximum), 0.70 D for both Q1 and Q3; and collision pressure, 1.5 mTorr.

For experiments conducted in SRM mode, a segmented tandem MS method was constructed based on the chromatographic retention times of the sphingolipids. For each class of sphingolipids such as ceramides and sphingomyelins, two or three methods were built, and, in each method, only five to six analyte SRM transitions were present that also included the respective ceramide or sphingomyelin internal standard precursor-to-product ion transitions. Experiments were performed in triplicate. Data acquisition and analysis were accomplished using Xcalibur software version 2.0.5 (Thermo Electron Corp.).

Quantitation data were corrected for the carbon number difference between a given molecular species and the selected internal standard (different in degrees because of varying carbon chain lengths, which results in different ionization efficiencies) according to the following formula (Han and Gross, 2005): $z1 = (1 + 0.011n + 0.0112n\,(n - 1)/2)/(1 + 0.011s + 0.0112s\,(s - 1)/2)$.

Antibodies

The following antibodies were used: mouse monoclonal antiactin (AC-15), rabbit polyclonal anti–calnexin ER marker, chicken polyclonal anti-COL4A3BP (M-150), secondary antibody goat anti–chicken IgY, HRP linked (Abcam), rabbit polyclonal anti-Akt, phospho-Akt (Ser473), CDC-2, phospho–CDC-2 (Tyr15), phospho-GSK-3–β (Ser9), phenylenediamine, phospho-PDK1 (Ser241), phospho-PTEN (Ser380), phospho–p44/42 MAPK (Thr/Tyr204), phospho–stress-activated protein kinase/JNK (Thr/Tyr185), phospho–p38 MAPK (Thr180/Tyr182), rabbit monoclonal anti-BiP (9C50B12), IRE1A (14C10), phospho-PERK, secondary antibody anti–rabbit IgG, HRP linked (Cell Signaling Technology), rabbit polyclonal anti-ATF4 (ProteinTech Group, Inc.), rabbit polyclonal anti-ATF6 (AnaSpec), mouse monoclonal anti-Bak (Ab-2), rabbit polyclonal anti-Bax (Ab-1), Bcl-2 (Ab-2), Bcl-x (Ab-1; EMD), mouse monoclonal anti–cyclin B (Invitrogen), rabbit polyclonal anti–cyclin D1 (Thermo Fisher Scientific), mouse monoclonal anti–cytochrome *c* (Assay Designs), rabbit monoclonal anti-phospho–eIF2-α (pS51; Epitomics), mouse monoclonal anti–GADD 153 (B-3), secondary antibody goat anti–mouse IgG, and HRP linked (Santa Cruz Biotechnology, Inc.). Kaleidoscope prestained standards were purchased from Bio-Rad Laboratories, and molecular weight standards were purchased from Santa Cruz Biotechnology, Inc.

Immunoblotting

Immunoblot analysis of cell protein lysates was performed according to the instructions of Santa Cruz Biotechnology, Inc. In brief, frozen tissue (embryos) was thawed in ice-cold radio immunoprecipitation assay buffer with freshly added inhibitors (1× PBS, 1% Igepal, 0.5% sodium deoxycholate, 0.1% SDS, 10 mg/ml PMSF, 50 mg/ml aprotinin, and 1 mmol/liter sodium orthovanadate [Sigma-Aldrich]) and homogenized on ice with a polytron device followed by centrifugation at 10,000 *g* for 20 min at 4°C. The concentration of supernatant protein was quantified using protein assay (Bio-Rad Laboratories). Samples were mixed with 2× Laemmli buffer (Bio-Rad Laboratories) and denatured at 100°C for 5 min, and 50 µg of denatured protein per lane was separated by NuPAGE 4–12% Bis-Tris gel (Invitrogen). Separated proteins were transferred to polyvinylidene difluoride membrane (Millipore) and subjected to immunoblotting with various primary antibodies. Positive antibody reactions were visualized with an HRP-conjugated secondary antibody and a chemiluminescence detection system (PerkinElmer) according to the manufacturer's instruction. The membrane was deprobed and reprobed with an antiactin antibody to confirm that all samples contained similar amounts of proteins. TTBS (TBS with 0.05% Tween 20) was used as a washing buffer, and 5% nonfat dry milk (Bio-Rad Laboratories) was dissolved in TTBS and used as a blocking solution.

RT-PCR analysis

Total RNA was extracted using the TRIZOL reagent (Invitrogen), and cDNAs were generated with reverse transcription (SuperScriptII; Invitrogen) according to the manufacturer's instructions. 2 µl cDNA was amplified in the PCR Master Mix solution (Promega).

Online supplemental material

Fig. S1 shows that the gene trap vector efficiently traps the *Cert* gene. Fig. S2 shows EM evidence of defects in the ER and mitochondria in cells from the developing embryonic optic cup of $Cert^{gt/gt}$ embryos. Fig. S3 shows that ER and mitochondrial defects can be noticed even at E9.5. Fig. S4 shows that blastocysts from the preimplantation stage do not show gross abnormalities. Fig. S5 shows that $Cert^{gt/gt}$-derived primary MEFs are capable of undergoing apoptosis. Videos 1 and 2 compare the cardiac output from E10.5 embryos of $Cert^{+/+}$ and $Cert^{gt/gt}$, demonstrating the circulation defects in the mutant heart. Table S1 shows the detailed quantification of the different species of sphingomyelin and ceramides estimated in the whole embryos and plasma membrane preparations of $Cert^{+/+}$ and $Cert^{gt/gt}$ at E10.5. Online supplemental material is available at http://www.jcb.org/cgi/content/full/jcb.200807176/DC1.

We thank BayGenomics for making the CERT gene trap insertion line available. We also wish to thank Drs. Shyam Sharan and Ira Daar for helpful discussions and critical reading of the manuscript. Dr. Shyam Sharan's guidance for mouse methodologies is gratefully acknowledged.

This work was supported by the Intramural Research Program of the National Cancer Institute, National Institutes of Health, and Department of Health and Human Services. U. Acharya is supported by a grant from the National Institutes of Health (R01EY16469).

Submitted: 29 July 2008
Accepted: 3 December 2008

References

Acharya, U., and J.K. Acharya. 2005. Enzymes of sphingolipid metabolism in *Drosophila melanogaster*. *Cell. Mol. Life Sci.* 62:128–142.

Acharya, U., M.B. Edwards, R.A. Jorquera, H. Silva, K. Nagashima, P. Labarca, and J.K. Acharya. 2006. *Drosophila melanogaster* Scramblases modulate synaptic transmission. *J. Cell Biol.* 173:69–82.

Alvarez, S.E., S. Milstien, and S. Spiegel. 2007. Autocrine and paracrine roles of sphingosine-1-phosphate. *Trends Endocrinol. Metab.* 18:300–307.

Berthet, C., and P. Kaldis. 2007. Cell-specific responses to loss of cyclin-dependent kinases. *Oncogene*. 26:4469–4477.

Bertolotti, A., X. Wang, I. Novoa, R. Jungreis, K. Schlessinger, J.H. Cho, A.B. West, and D. Ron. 2001. Increased sensitivity to dextran sodium sulfate colitis in IRE1beta-deficient mice. *J. Clin. Invest.* 107:585–593.

Bionda, C., J. Portoukalian, D. Schmitt, C. Rodriguez-Lafrasse, and D. Ardail. 2004. Subcellular compartmentalization of ceramide metabolism: MAM (mitochondria-associated membrane) and/or mitochondria? *Biochem. J.* 382:527–533.

Bozidis, P., C.D. Williamson, and A.M. Colberg-Poley. 2007. Isolation of endoplasmic reticulum, mitochondria, and mitochondria-associated membrane fractions from transfected cells and from human cytomegalovirus-infected primary fibroblasts. *Curr. Protoc. Cell Biol.* Chapter 3:Unit 3.27.

Challice, C.E., and S. Viragh. 1974. The architectural development of the early mammalian heart. *Tissue Cell*. 6:447–462.

Copeland, D.E., and A.J. Dalton. 1959. An association between mitochondria and the endoplasmic reticulum in cells of the pseudobranch gland of a teleost. *J. Biophys. Biochem. Cytol.* 5:393–396.

Csordas, G., C. Renken, P. Varnai, L. Walter, D. Weaver, K.F. Buttle, T. Balla, C.A. Mannella, and G. Hajnoczky. 2006. Structural and functional features and significance of the physical linkage between ER and mitochondria. *J. Cell Biol.* 174:915–921.

Datta, B., R. Datta, A. Majumdar, and A. Ghosh. 2005. The stability of eukaryotic initiation factor 2-associated glycoprotein, p67, increases during skeletal

muscle differentiation and that inhibits the phosphorylation of extracellular signal-regulated kinases 1 and 2. *Exp. Cell Res.* 303:174–182.

Eggens, I., C. Valtersson, G. Dallner, and L. Ernster. 1979. Transfer of phospholipids between the endoplasmic reticulum and mitochondria in rat hepatocytes in vivo. *Biochem. Biophys. Res. Commun.* 91:709–714.

English, D., D.N. Brindley, S. Spiegel, and J.G. Garcia. 2002. Lipid mediators of angiogenesis and the signalling pathways they initiate. *Biochim. Biophys. Acta*. 1582:228–239.

Ermonval, M., R. Cacan, K. Gorgas, I.G. Haas, A. Verbert, and G. Buttin. 1997. Differential fate of glycoproteins carrying a monoglucosylated form of truncated N-glycan in a new CHO line, MadIA214214, selected for a thermosensitive secretory defect. *J. Cell Sci.* 110:323–336.

Eroglu, C., B. Brugger, F. Wieland, and I. Sinning. 2003. Glutamate-binding affinity of *Drosophila* metabotropic glutamate receptor is modulated by association with lipid rafts. *Proc. Natl. Acad. Sci. USA*. 100:10219–10224.

Franzini-Armstrong, C. 2007. ER-mitochondria communication. How privileged? *Physiology (Bethesda)*. 22:261–268.

Fukasawa, M., M. Nishijima, and K. Hanada. 1999. Genetic evidence for ATP-dependent endoplasmic reticulum-to-Golgi apparatus trafficking of ceramide for sphingomyelin synthesis in Chinese hamster ovary cells. *J. Cell Biol.* 144:673–685.

Futerman, A.H., and Y.A. Hannun. 2004. The complex life of simple sphingolipids. *EMBO Rep.* 5:777–782.

Haberkant, P., O. Schmitt, F.X. Contreras, C. Thiele, K. Hanada, H. Sprong, C. Reinhard, F.T. Wieland, and B. Brugger. 2008. Protein-sphingolipid interactions within cellular membranes. *J. Lipid Res.* 49:251–262.

Han, X., and R.W. Gross. 2005. Shotgun lipidomics: electrospray ionization mass spectrometric analysis and quantitation of cellular lipidomes directly from crude extracts of biological samples. *Mass Spectrom. Rev.* 24:367–412.

Hanada, K. 2006. Discovery of the molecular machinery CERT for endoplasmic reticulum-to-Golgi trafficking of ceramide. *Mol. Cell. Biochem.* 286:23–31.

Hanada, K., K. Kumagai, S. Yasuda, Y. Miura, M. Kawano, M. Fukasawa, and M. Nishijima. 2003. Molecular machinery for non-vesicular trafficking of ceramide. *Nature*. 426:803–809.

Hannun, Y.A., and L.M. Obeid. 2008. Principles of bioactive lipid signalling: lessons from sphingolipids. *Nat. Rev. Mol. Cell Biol.* 9:139–150.

Hetz, C., P. Bernasconi, J. Fisher, A.H. Lee, M.C. Bassik, B. Antonsson, G.S. Brandt, N.N. Iwakoshi, A. Schinzel, L.H. Glimcher, and S.J. Korsmeyer. 2006. Proapoptotic BAX and BAK modulate the unfolded protein response by a direct interaction with IRE1alpha. *Science*. 312:572–576.

Hla, T. 2005. Genomic insights into mediator lipidomics. *Prostaglandins Other Lipid Mediat.* 77:197–209.

Karbowski, M., K.L. Norris, M.M. Cleland, S.Y. Jeong, and R.J. Youle. 2006. Role of Bax and Bak in mitochondrial morphogenesis. *Nature*. 443:658–662.

Kawano, M., K. Kumagai, M. Nishijima, and K. Hanada. 2006. Efficient trafficking of ceramide from the endoplasmic reticulum to the Golgi apparatus requires a VAMP-associated protein-interacting FFAT motif of CERT. *J. Biol. Chem.* 281:30279–30288.

Liu, M., E.S. Krul, and P.V. Subbaiah. 1992. Effect of apoprotein B conformation on the activation of lysolecithin acyltransferase and lecithin: cholesterol acyltransferase. Studies with subfractions of low density lipoproteins. *J. Biol. Chem.* 267:5139–5147.

Malhotra, J.D., and R.J. Kaufman. 2007. Endoplasmic reticulum stress and oxidative stress: a vicious cycle or a double-edged sword? *Antioxid. Redox Signal.* 9:2277–2293.

Meier, P.J., M.A. Spycher, and U.A. Meyer. 1978. Isolation of a subfraction of rough endoplasmic reticulum closely associated with mitochondria. Evidence for its role in cytochrome P450 synthesis. *Exp. Cell Res.* 111:479–483.

Menaldino, D.S., A. Bushnev, A. Sun, D.C. Liotta, H. Symolon, K. Desai, D.L. Dillehay, Q. Peng, E. Wang, J. Allegood, et al. 2003. Sphingoid bases and de novo ceramide synthesis: enzymes involved, pharmacology and mechanisms of action. *Pharmacol. Res.* 47:373–381.

Merrill, A.H. Jr. 2002. De novo sphingolipid biosynthesis: a necessary, but dangerous, pathway. *J. Biol. Chem.* 277:25843–25846.

Merrill, A.H. Jr., M.C. Sullards, J.C. Allegood, S. Kelly, and E. Wang. 2005. Sphingolipidomics: high-throughput, structure-specific, and quantitative analysis of sphingolipids by liquid chromatography tandem mass spectrometry. *Methods*. 36:207–224.

Morre, D.J., W.D. Merritt, and C.A. Lembi. 1971. Connections between mitochondria and endoplasmic reticulum in rat liver and onion stem. *Protoplasma*. 73:43–49.

Oakes, S.A., S.S. Lin, and M.C. Bassik. 2006. The control of endoplasmic reticulum-initiated apoptosis by the BCL-2 family of proteins. *Curr. Mol. Med.* 6:99–109.

Ogretmen, B., and Y.A. Hannun. 2004. Biologically active sphingolipids in cancer pathogenesis and treatment. *Nat. Rev. Cancer*. 4:604–616.

Parrinello, S., E. Samper, A. Krtolica, J. Goldstein, S. Melov, and J. Campisi. 2003. Oxygen sensitivity severely limits the replicative lifespan of murine fibroblasts. *Nat. Cell Biol.* 5:741–747.

Rao, R.P., C. Yuan, J.C. Allegood, S.S. Rawat, M.B. Edwards, X. Wang, A.H. Merrill Jr., U. Acharya, and J.K. Acharya. 2007. Ceramide transfer protein function is essential for normal oxidative stress response and lifespan. *Proc. Natl. Acad. Sci. USA*. 104:11364–11369.

Reimold, A.M., A. Etkin, I. Clauss, A. Perkins, D.S. Friend, J. Zhang, H.F. Horton, A. Scott, S.H. Orkin, M.C. Byrne, et al. 2000. An essential role in liver development for transcription factor XBP-1. *Genes Dev.* 14:152–157.

Riezman, H. 2006. Organization and functions of sphingolipid biosynthesis in yeast. *Biochem. Soc. Trans.* 34:367–369.

Rizzuto, R., M.R. Duchen, and T. Pozzan. 2004. Flirting in little space: the ER/mitochondria Ca2+ liaison. *Sci. STKE*. doi:10.1126/stke.2152004re1.

Ron, D., and P. Walter. 2007. Signal integration in the endoplasmic reticulum unfolded protein response. *Nat. Rev. Mol. Cell Biol.* 8:519–529.

Ruby, J.R., R.F. Dyer, and R.G. Skalko. 1969. Continuities between mitochondria and endoplasmic reticulum in the mammalian ovary. *Z. Zellforsch. Mikrosk. Anat.* 97:30–37.

Rutkowski, D.T., S.M. Arnold, C.N. Miller, J. Wu, J. Li, K.M. Gunnison, K. Mori, A.A. Sadighi Akha, D. Raden, and R.J. Kaufman. 2006. Adaptation to ER stress is mediated by differential stabilities of pro-survival and pro-apoptotic mRNAs and proteins. *PLoS Biol.* 4:e374.

Satyanarayana, A., M.B. Hilton, and P. Kaldis. 2008. p21 inhibits Cdk1 in the absence of Cdk2 to maintain the G1/S phase DNA damage checkpoint. *Mol. Biol. Cell*. 19:65–77.

Savtchouk, I.A., F.J. Mattie, and A.A. Ollis. 2007. Ceramide: from embryos to tumors. *Sci. STKE*. doi:10.1126/stke.3942007jc1.

Scheuner, D., and R.J. Kaufman. 2008. The unfolded protein response: a pathway that links insulin demand with beta-cell failure and diabetes. *Endocr. Rev.* 29:317–333.

Scheuner, D., D. Vander Mierde, B. Song, D. Flamez, J.W. Creemers, K. Tsukamoto, M. Ribick, F.C. Schuit, and R.J. Kaufman. 2005. Control of mRNA translation preserves endoplasmic reticulum function in beta cells and maintains glucose homeostasis. *Nat. Med.* 11:757–764.

Shore, G.C., and J.R. Tata. 1977. Two fractions of rough endoplasmic reticulum from rat liver. I. Recovery of rapidly sedimenting endoplasmic reticulum in association with mitochondria. *J. Cell Biol.* 72:714–725.

Sissman, N.J. 1970. Developmental landmarks in cardiac morphogenesis: comparative chronology. *Am. J. Cardiol.* 25:141–148.

Stryke, D., M. Kawamoto, C.C. Huang, S.J. Johns, L.A. King, C.A. Harper, E.C. Meng, R.E. Lee, A. Yee, L. L'Italien, et al. 2003. BayGenomics: a resource of insertional mutations in mouse embryonic stem cells. *Nucleic Acids Res.* 31:278–281.

Subbaiah, P.V., and M. Liu. 1993. Role of sphingomyelin in the regulation of cholesterol esterification in the plasma lipoproteins. Inhibition of lecithin-cholesterol acyltransferase reaction. *J. Biol. Chem.* 268:20156–20163.

Sussman, M. 2007. "AKT"ing lessons for stem cells: regulation of cardiac myocyte and progenitor cell proliferation. *Trends Cardiovasc. Med.* 17:235–240.

Swanton, C., M. Marani, O. Pardo, P.H. Warne, G. Kelly, E. Sahai, F. Elustondo, J. Chang, J. Temple, A.A. Ahmed, et al. 2007. Regulators of mitotic arrest and ceramide metabolism are determinants of sensitivity to paclitaxel and other chemotherapeutic drugs. *Cancer Cell*. 11:498–512.

Tinton, S.A., B. Schepens, Y. Bruynooghe, R. Beyaert, and S. Cornelis. 2005. Regulation of the cell-cycle-dependent internal ribosome entry site of the PITSLRE protein kinase: roles of Unr (upstream of N-ras) protein and phosphorylated translation initiation factor eIF-2alpha. *Biochem. J.* 385:155–163.

Travers, K.J., C.K. Patil, L. Wodicka, D.J. Lockhart, J.S. Weissman, and P. Walter. 2000. Functional and genomic analyses reveal an essential coordination between the unfolded protein response and ER-associated degradation. *Cell*. 101:249–258.

Umebayashi, K., A. Hirata, R. Fukuda, H. Horiuchi, A. Ohta, and M. Takagi. 1997. Accumulation of misfolded protein aggregates leads to the formation of russell body-like dilated endoplasmic reticulum in yeast. *Yeast*. 13:1009–1020.

van Anken, E., and I. Braakman. 2005. Endoplasmic reticulum stress and the making of a professional secretory cell. *Crit. Rev. Biochem. Mol. Biol.* 40:269–283.

van Meer, G., and Q. Lisman. 2002. Sphingolipid transport: rafts and translocators. *J. Biol. Chem.* 277:25855–25858.

van Meer, G., D.R. Voelker, and G.W. Feigenson. 2008. Membrane lipids: where they are and how they behave. *Nat. Rev. Mol. Cell Biol.* 9:112–124.

Vance, J.E. 1991. Newly made phosphatidylserine and phosphatidylethanolamine are preferentially translocated between rat liver mitochondria and endoplasmic reticulum. *J. Biol. Chem.* 266:89–97.

Viragh, S., and C.E. Challice. 1973. Origin and differentiation of cardiac muscle cells in the mouse. *J. Ultrastruct. Res.* 42:1–24.

Wei, M.C., W.X. Zong, E.H. Cheng, T. Lindsten, V. Panoutsakopoulou, A.J. Ross, K.A. Roth, G.R. MacGregor, C.B. Thompson, and S.J. Korsmeyer. 2001. Proapoptotic BAX and BAK: a requisite gateway to mitochondrial dysfunction and death. *Science*. 292:727–730.

Wu, J., and R.J. Kaufman. 2006. From acute ER stress to physiological roles of the Unfolded Protein Response. *Cell Death Differ.* 13:374–384.

Zeidan, Y.H., and Y.A. Hannun. 2007. Translational aspects of sphingolipid metabolism. *Trends Mol. Med.* 13:327–336.

Zhang, K., H.N. Wong, B. Song, C.N. Miller, D. Scheuner, and R.J. Kaufman. 2005. The unfolded protein response sensor IRE1alpha is required at 2 distinct steps in B cell lymphopoiesis. *J. Clin. Invest.* 115:268–281.

Zheng, W., J. Kollmeyer, H. Symolon, A. Momin, E. Munter, E. Wang, S. Kelly, J.C. Allegood, Y. Liu, Q. Peng, et al. 2006. Ceramides and other bioactive sphingolipid backbones in health and disease: lipidomic analysis, metabolism and roles in membrane structure, dynamics, signaling and autophagy. *Biochim. Biophys. Acta*. 1758:1864–1884.